Journal of Mineralogical and Petrological Sciences, Volume 100, page 247–259, 2005

X-ray studies of structural changes in melanophlogite with varying temperature

Takeshi NAKAGAWA[*,***], Kuniaki KIHARA[*] and Syuhei FUJINAMI[**]

[*]*Department of Earth Sciences, Kanazawa University, Kakuma, Kanazawa 920-1192, Japan*
[**] *Department of Chemistry, Kanazawa University, Kakuma, Kanazawa 920-1192, Japan*
[***] *Present address: Toray Research Center, Inc, Sono-yama, Otsu 520-8567, Japan*

The *a* and *c* unit cell dimensions of melanophlogite (MEP) have been determined in the temperature range −50 to 700 °C, showing a different expansion behavior for the low temperature α-phase. The *c*-axis length, 2*c*, which is smaller than *a*-axis length in the α-phase, shows a steep rise reaching the value of *a* at the tetragonal (α)-cubic (β) transition temperature at about 65 °C, and then remains nearly constant until about 500 °C, after which contraction occurs. The crystal structures of α-MEP (space group = $P4_2/nbc$) and β-MEP (space group = $Pm\bar{3}n$) were refined using a least-squares refinement of a harmonic structure factor expression, using single crystal X-ray diffraction data measured at seven temperatures from −50 to 200 ºC (four points for the α-phase, and three points for the β-phase). The average Si-O distance decreased from 1.593 Å at −50 °C down to 1.573 Å at 63 °C (the estimated transition point). It then remained nearly constant in the β-phase. The Si-O bond distance corrected using a simple rigid body motion model remained nearly constant at 1.611 Å in the temperature range −50 to 200 °C, indicating that the negative temperature dependence is due to strong distortions of the probability density functions of the O atoms. The atomic mean-square displacement, $\langle u^2 \rangle$, of the O atoms increased steeply with increasing temperature up to the α-β transition point. The low-high (α-β) transformation in MEP is driven by a mechanism involving atom disorder beginning in the low-temperature phase.

Keywords: Melanophlogite, Atomic mean-square displacements, α-β transition, X-ray structural analysis, Temperature dependence

INTRODUCTION

Materials containing large free spaces for guest molecules have been the subject of a variety of studies, because of their high possibilities in applications. So far, many types of silica clathrates containing different types of polyhedral voids have been reported, mainly in relation to their synthesis with various guest molecules (Gies and Marler, 1992). The mineral melanophlogite (MEP) occurs among these silica clathrates, and has the chemical formula $46SiO_2 \cdot 2M^{12} \cdot 6M^{14}$, where M^{12} denotes pentagondodecahedral voids and M^{14} denotes tetrakaidecahedral voids. The M^{12} cage usually contains molecules such as CH_4 and N_2, and the M^{14} voids contain molecules such as CO_2, and N_2. Since the first description of MEP as a new mineral from Sicilian sulfur deposits, many structural studies have been carried out using microscopic, spectroscopic, and X-ray diffraction techniques (Skinner and Appleman, 1963; Kamb, 1965; Žák, 1972; Gies, 1983; Kortus et al., 2000; Nakagawa et al., 2001; Nakagawa, 2002). However, some important structural details of this mineral and corresponding synthetic materials remain to be determined, particularly the details of the temperature dependency of the structure, the structural behavior of guest molecules, and their effect on the stability of these low density (e.g., 2.0×10^3 kg/m^3) frameworks.

Two phases are known to exist above room temperature for MEP. According to the literature, the β-phase is cubic with space group $Pm\bar{3}n$ (Gies, 1983), and the α-phase, a ($2 \times 2 \times 1$) superstructure of the β-form, is tetragonal with space group $P4_2/nbc$ (Žák, 1972; Nakagawa et al. 2001). Samples from Mt. Hamilton (California, USA) show a tetragonal-cubic phase transition at 65 °C (Gies, 1983). The relationships between the atom sites for both phases are summarized in Table 1. Twelve independent O atoms, O_1 to O_{12}, in the α-phase become equivalent in the β-phase. These O atoms are denoted as Group O_1. Similarly, the six O_{13} to O_{18} atoms are denoted as Group O_2, the four O atoms from O_{19} to O_{22} are denoted as Group O_3, and the final three O atoms from O_{23} to O_{25}

K. Kihara kuniaki@kenroku.kanazawa-u.ac.jp Corresponding author

Table 1. Equivalent atomic sites in α- and β-melanophlogites, $46SiO_2 \cdot 2M^{12} \cdot 6M^{14}$ *1

α-melanophlogite $P4_2/nbc$ (No.133), $Z = 4$ $a = 26.818(2)$, $c = 13.365(1)$ Å at 25 °C (Nakagawa et al., 2001)		β-melanophlogite $a = 13.4104(9)$ Å at 84 °C, $Z = 1$			
		$Pm\bar{3}n$ (No. 223)		$P\bar{4}3n$ (No. 218)	
Atomic sites	N W S*2	Atomic sites	N W S*2	Atomic sites	N W S*2
Si_1-Si_6	16 k 1 × 6	Si_1	24 k *m*..	Si_1	24 i 1
Si_7-Si_{10}	16 k 1 × 4	Si_2	16 i .3.	Si_{21} Si_{22}	8 e .3. 8 e .3.
Si_{11},Si_{12} Si_{13}	8 i .2. × 2 8 j ..2 × 1	Si_3	6 c 4*m*.2	Si_3	6 d $\bar{4}$..
O_1-O_{12}	16 k 1 × 12	O_1	48 l 1	O_{11} O_{12}	24 i 1 24 i 1
O_{13}-O_{18}	16 k 1 × 6	O_2	24 k *m*..	O_2	24 i 1
O_{19}, O_{20} O_{21}, O_{22}	8 h .2. × 2 16 k 1 × 2	O_3	12 f *mm*2..	O_3	12 f 2..
O_{23} O_{24}, O_{25}	16 k 1 × 1 8 j ..2 × 2	O_4	8 e .32	O_4	8 4 .3.
M^{14} (1) M^{14} (2) M^{14} (3)	4 d $\bar{4}$.. × 1 4 c 222 × 1 16 k 1 × 1	M^{14}	6 d 4*m*.2	M^{14}	6 c $\bar{4}$..
M^{12}	8 h .2. × 1	M^{12}	2 a $m\bar{3}$.	M^{12}	2 a 23.

Note:Origin of α-melanophlogite on 222, at $(\bar{1}/4, \bar{1}/4, 0)$ from $\bar{1}$.

*1 M^{12} : pentagondodecahedral site, may contain CH_4 or N_2, M^{14}: tetrakaidecahedral site, may contain CO_2 or N_2 etc.

*2 N, W and S: Number of equivalent positions, Wyckoff notation and site symmetry, respectively.

are denoted as Group O_4.

The characteristic features of the structural refinement of the β-phase of MEP show highly anisotropic and large-magnitude mean-square displacements (MSDs), particularly for the O atoms, with a short Si-O bond distance (1.576 Å) and a large Si-O-Si bond angle (168.8°) compared with the bond lengths and angles of common silica polymorphs (Gies, 1983). According to this author, the MSDs of the framework O atoms in this phase are the result of a considerable contribution from static or dynamic disorder.

In the structural refinement of some silica polymorphs, the Si-O bond distances calculated from the atomic mean positions tend to decrease with increasing temperature, being associated with increasing anisotropy and the magnitude of the MSDs of the O atoms (Kihara, 1990; Kihara et al., 1986; Downs et al., 1990; Downs et al., 1992). The increase in MSDs at high temperatures is far above that expected from pure thermal vibrations (by phonon modes) in some cases. Examples are seen in tridymite (Kihara et al. 1986; Hirose et al., 2005), and cristobalite (Peacor, 1973; Wright and Leadbetter, 1975; Hatch and Ghose, 1991). This study focused on the temperature dependence of the unit-cell dimensions, atomic positional parameters, and MSDs of the framework atoms in MEP.

EXPERIMENTAL

Transparent crystalline samples of natural MEP from Mt. Hamilton were obtained from Rogers Minerals (Ontario, Canada). Three fragments were used as samples in our X-ray studies, denoted as Samples 1230-02, 1230-09, and 00-88, with sizes of 0.17 × 0.17 × 0.15, 0.1 × 0.1 × 0.07, and 0.1 × 0.1 × 0.1 mm^3, respectively. From X-ray photographic data obtained at room temperature, all the samples, except Sample 00-88, were confirmed to be single-crystals exhibiting a tetragonal unit cell.

All the measurements above room temperature were performed using a four-circle diffractometer (Rigaku Model AFC7S, Japan) with an electric furnace, whose temperature was controlled using a PID controller with fluctuations < 1 °C up to a temperature of 200 °C, and ± 4 °C up to a temperature of 700 °C. The temperature was calibrated using the melting point of Sn (T_m = 227.968 °C), Pb (T_m = 327.5 °C), Zn (T_m = 419.58 °C), and Al (T_m = 660.37 °C). The measurements at –50 °C were performed

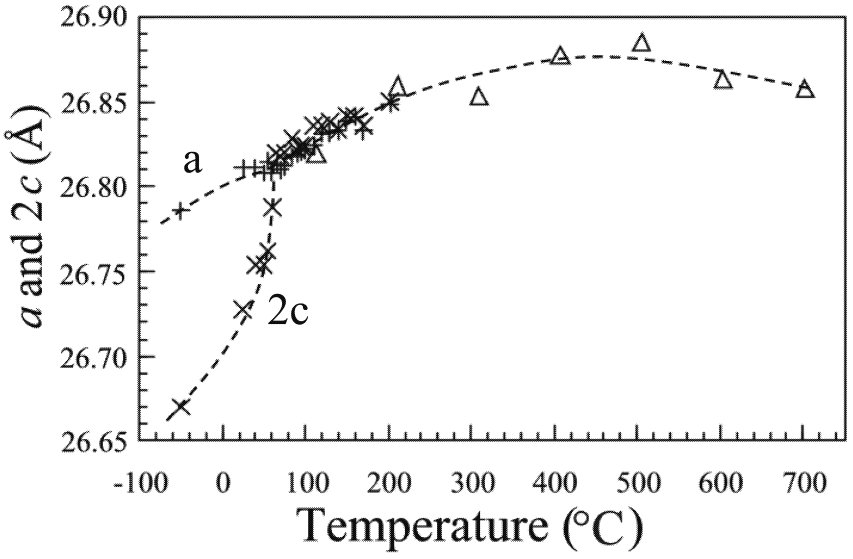

Figure 1. Temperature dependence of the unit cell dimensions of melanophlogite. The plus sign indicates *a*-axis dimensions measured on Sample 1230-02, and the crosses and open triangles denote the 2*c* values measured on Samples 1230-02 and 00-88, respectively. The broken lines are for visual guidance only.

Table 2. Unit-cell dimensions measured on specimens #1230-02 and #00-88

Temp (°C)	*a* (Å)	*c* (Å)
- 50	26.786(2)	13.3351(4)
25	26.811(2)	13.364(3)
40	26.811(2)	13.377(4)
50	26.808(2)	13.377(3)
55	26.815(2)	13.381(3)
60	26.808(3)	13.394(4)
65	26.813(3)	13.410(4)
70	26.810(3)	13.409(3)
75	26.812(3)	13.410(4)
84	13.4104(9)	
90	13.4100(9)	
95	13.4110(11)	
100	13.4111(9)	
	13.410(1)*	
110	13.4139(9)	
120	13.4163(9)	
130	13.4169(10)	
140	13.4165(9)	
150	13.4200(9)	
160	13.4207(10)	
170	13.4169(11)	
200	13.430(2)*	
202	13.4249(12)	
300	13.427(2)*	
400	13.439(4)*	
500	13.443(5)*	
600	13.432(3)*	
700	13.429(3)*	

* Measured on specimen #00-88

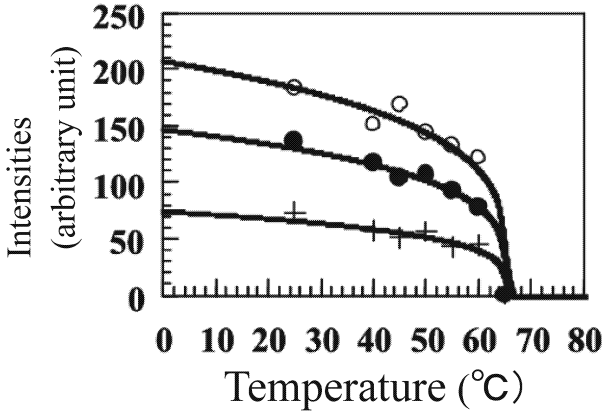

Figure 2. Integrated intensities of superstructure-reflections, 1$\underline{1}$01 (open circles), 383 (solid circles) and 5$\underline{1}$22 (crosses), all measured on Sample 1230-02, and the fit of their temperature dependences using a Landau expression. Parameters T_c and T_o were determined in a range 65.1 to 65.2 °C, and gaps in 1 to 2% of corresponding intensities at room temperature were observed at T_c.

using a CCD diffractometer (Rigaku, Japan) with a flowing N_2 gas cooling device, whose temperature was monitored and controlled to within ± 1 °C. All the measurements used graphite-monochromatized Mo *K*α radiation (λ = 0.71069 Å).

The unit-cell dimensions above room temperature were determined from least-squares fit of the θ values of 20 reflections in the range θ = 25 to 30°, whose peaks were measured in both the positive and negative ω, using a four-circle diffractometer for Sample 1230-02 from 25 to 202 °C and Sample 00-88 from 100 to 700°C. The resulting data, including those obtained from the CCD diffractometer at –50 °C, are tabulated in Table 2.

Figure 1 shows the temperature dependence of the cell dimensions: the *c*-axis dimension is doubled for comparison with the *a*-axis. The integrated intensities of the three strong superstructure reflections 1$\underline{1}$01, 383, and

5122 were also measured to monitor the effect of structural changes in the low temperature phase. Figure 2 shows the temperature evolution of the intensities of these reflections, measured on Sample 1230-02, together with the curves fitted to those data with a phenomenological equation applicable to first-order transitions as

$$Q(T) = \left(\frac{2}{3}\right)^{1/2} Q(T_c) \left[1 + \sqrt{1 - \frac{3(T - T_o)}{4(T_c - T_o)}}\right]^{1/2},$$

where Q is the order parameter of the transition, T_o the temperature at which the α- and β-phases have the same free energy, and T_c the temperature the free energy function is minimized at $Q = 0$ and $\pm Q(T_c)$. The best fitted curves, shown in Figure 2, were obtained from the variables, $T_c \approx T_o = 65.1$ to 65.2 °C, and $I(T_c)$ in 1 to 2% of the corresponding intensities at room temperature.

The integrated intensities of two samples were measured for the structural refinements: Sample 1230-09 for the measurements at –50 °C using the CCD diffractometer, and Sample 1230-02 at 25, 40, 60, 84, 100 and 200 °C on the four-circle diffractometer. The details of the experimental conditions of the intensity measurements are summarized in Table 3, together with some statistics of the refinements. The intensity data measured using the CCD diffractometer and the four-circle diffractometer were processed with the TEXSAN™ (1989) and the AFC7S software packages, respectively, to determine the structure factor amplitudes and their standard deviation. The space group of the α-phase was uniquely determined to be $P4_2/nbc$, as indicated by Nakagawa et al (2001), whereas the diffraction data allowed two possible space

Table 3. Data about intensity measurements and refinements

Radiation	Mo $K\alpha$					
μ (cm^{-1})	7.09					
(1) Measurement conditions on specimen #1230-09						
Temperature	-50°C					
Diffractometer	MercuryCCD (Rigaku)					
Ranges of measurements	h = -24 to 24, k = -34 to 34, ℓ = -16 to 16					
No. of reflections measured	33490					
No. of observed reflections[*1]	4363					
	0.039					
Parameters	334[*5]					
R[*3], R_w[*4]	0.052, 0.085					
(2) Measurement conditions on specimen #1230-02						
Temperatures (°C)	25	40	60	84	100	200
Diffractometer	4-circle diffractometer AFC7s (Rigaku)					
Parameters	338[*6]	335[*7]		37[1 + 1 + 9 + 26] [*8]	(55[1 + 1 + 16 + 37])[*9]	
Ranges of measurements	5≤2θ≤70°					
Reflection sphere measured[*2]	1/16				1/16	
No. of measured reflections	10211	10675	10794	2973	1805	2176
No. of observed reflections[*1]	3672	3818	3100	607	655	601
	-	-	-	0.028	0.026	0.021
R[*3]	0.060	0.056	0.071	0.040 0.037[*9]	0.045	0.039
R_w[*4]	0.066	0.060	0.075	0.047 0.042[*9]	0.054	0.045

[*1] Number of symmetry independent reflections satisfying $F_o \geq 3\sigma(F_o)$, associated by $R_{int} = \Sigma(|F_j| - |F_{ave}|)/\Sigma|F_{ave}|$, if those are averaged over equivalent reflections.

[*2] Measured region in fraction to the reflection sphere.

[*3] $R = \Sigma||F_O| - |F_C||/\Sigma F_O$, [*4] $R_w = \{\Sigma[w(F_O - |F_C|)^2]/\Sigma wF_O^2\}^{1/2}$

[*5] Number of parameters including 1 scale factor (abbreviated as sf), 104 positional parameters (pp) and 229 anisotropic temperature factors (atf).

[*6] Number of parameters including 1 sf, 1 isotropic extinction factor (ief), 3 atom multiplicities (am) for M^{12}, $M^{14}(1)$, $M^{14}(3)$ and $M^{14}(4)$, 104 pps and 229 atfs.

[*7] Number of parameters including 1 sf, 1 ief, 104 pps and 229 atfs. Ams for the M sites were fixed on those for 25 °C.

[*8] Number of parameters including 1 sf, 1 ief, 9 pps and 26 atfs.

[*9] For space group $P\bar{4}3n$. Parameters include 1 sf, 1 ief, 16 pps and 37 atfs.

groups, $Pm\bar{3}n$ and $P\bar{4}3n$, for the β-phase, i.e., the Laue symmetry of the β-phase was confirmed to be $m\bar{3}m$ in the measured intensity distribution, but the systematic absences observed for the $hh\ell$ and 00ℓ reflections for odd ℓ allow for two space groups. The standard deviation of each observed structure amplitude, F_o, was estimated from the counting statistics. When measured, the symmetry-equivalent reflections (see Table 3) were summed to give an averaged F_o, and their standard deviation was estimated from their own dispersion for use in the least-squares refinements. All reflections satisfying the condition, $F_o \geq 3\sigma(F_o)$, were assumed to be observed.

LEAST-SQUARES REFINEMENT

According to Gies (1983), molecular methane, carbon dioxide, and nitrogen guest molecules can be accommodated in the M^{12} and M^{14} sites in a crystal from Mt. Hamilton. Gies (1983) estimated from the experimental data (mass spectroscopy and X-ray least-squares refinements) that the M^{12} and M^{14} sites contain 9 and 12 electrons per cage, respectively. Our preliminary molecular dynamics simulation shows that those guest molecules move around inside the cages in a random manner. In the present study, the least-squares refinement was attempted using spherical form factors for substitute atoms in the M^{12} and M^{14} sites, expecting a population density of 100% to correspond to scattering for each site. F and Mg were used as the substitute atoms, by taking into account the number of their electrons. Neutral atomic scattering factors and the anomalous dispersions of Cromer and Waber (1974) were used for these substitute and the framework atoms, respectively. The quantity $\Sigma w(F_o - k|F_c|)^2$ was minimized with $w = 1/\sigma^2(F_o)$, where k is a scale factor and σ is the estimated standard deviation of F_o.

The tetragonal unit cell of α-MEP contains 584 atoms (or sites), which are divided into 42 symmetry-independent groups. By including a scale factor, an isotropic extinction factor (Becker and Coppens, 1974), and four site occupancy factors for the M^{14} and M^{12} sites, we have 339 variables for refinement with anisotropic temperature factors. The least-squares calculations initiated using the room temperature atomic parameters of Nakagawa et al. (2001) converged to R-factors in the range R = 0.05-0.07 at four different temperatures. The population densities for $M^{14}(1)$, $M^{14}(2)$, $M^{14}(3)$, and M^{12} in the room temperature refinement were 0.85(14), 1.04(12), 0.92(4), and 0.73(4), respectively, which correspond to population densities of 0.93 for M^{14} and 0.73 for M^{12} in the β-phase (full occupation = 1). These results suggest that the number of electrons in, at least, the three symmetrically independent cage sites $M^{14}(1)$, $M^{14}(3)$, and M^{12} are less than expected from the results of Gies (1983).

The cubic unit cell of β-MEP contains 146 atoms (or sites), which are divided into nine symmetry-independent groups in the case of space group $Pm\bar{3}n$. In total, 39 variables (a scale factor, an isotropic extinction factor, and the 37 atomic parameters including anisotropic temperature factor coefficients and the multiplicities of the M^{12} and M^{14} sites) were fitted using least squares calculations initiated with the parameters of Gies (1983). The refinement of the site occupancy factors of the M^{12} and M^{14} sites resulted in population densities of 0.77(5) and 0.98(7), respectively. The values of the refined population densities for 25 and 84 °C agree within one estimated standard deviation (esd) suggesting that the guest molecules remain in their cages at these temperatures. In this work, data obtained with the multiplicities fixed on these values is presented. The refinements resulted in a smooth convergence, R-factors = 0.04-0.05, of the variable parameters into near constant values, giving rise to interpretable atomic distances at these three temperatures. The difference Fourier syntheses show negative values at all the O atom sites surrounded by positive contours, suggesting that the O atoms undergo highly anharmonic thermal vibrations or that atom disordering occurs at the O atom sites. The fractional coordinates and equivalent isotropic temperature factors are tabulated in Table 4 for selected cases: –50 and 60 °C for the α-phase, and 84 °C for the β-phase. As usual, the present coordinates and temperature factors may represent unbiased estimates of the mean and dispersion of the general probability density functions (PDFs) of the atoms (Mair and Wilkins, 1981). The Si-O bond lengths and Si-O-Si angles calculated using the present coordinates and unit-cell dimensions are shown in Tables 5. The projections of the structures on the (001) plane, drawn using the final parameters, are shown in Figure 3. More detailed structural data is available on request from the authors.

For space group $P\bar{4}3n$, the atoms in the β-phase can be grouped into eleven independent sets with 57 variable parameters (a scale, an isotropic extinction factor, and 55 atomic parameters including anisotropic temperature factor coefficients). The least-squares refinements were attempted at three temperatures, and all resulted to R-factors lower than those for the $Pm\bar{3}n$ space group (Table 3), but with position parameters that gave rise to larger dispersions of the Si-O bond distances, which was not consistent throughout the three temperatures. As discussed later, the present study strongly suggests that the α-phase is increasingly subjected to framework atom disorder over the multiple potential energy minima with increasing temperature, and this disorder finally leads to the α-β structural transition. According to Nakagawa and Kihara

Table 4. Fractional coordinates and equivalent temperature factors at –50, 60 and 84 °C

	– 50 °C				60 °C			
atom	x	y	z	B_{eq}(Å^2)	x	y	z	B_{eq}(Å^2)
Si_1	0.19249(4)	0.01001(4)	0.30891(8)	1.12(2)	0.1918(3)	0.0066(2)	0.3088(6)	1.77(9)
Si_2	0.30704(4)	0.00665(4)	0.31037(8)	1.07(2)	0.3062(2)	0.0043(1)	0.3108(5)	1.02(7)
Si_3	0.09522(4)	0.05767(4)	– 0.00284(8)	1.15(3)	0.0947(3)	0.0565(3)	– 0.0024(3)	2.40(14)
Si_4	0.40603(4)	0.05733(4)	– 0.00582(8)	1.17(2)	0.4052(2)	0.0576(2)	– 0.0046(2)	0.84(9)
Si_5	0.25381(4)	0.16044(4)	0.09601(8)	0.97(2)	0.2494(2)	0.1580(1)	0.1052(2)	1.45(6)
Si_6	0.24685(4)	0.15255(4)	0.86840(8)	1.04(2)	0.2452(2)	0.1529(1)	0.8772(2)	1.05(5)
Si_7	0.16063(4)	0.09860(4)	0.17043(8)	1.07(2)	0.1600(2)	0.0949(2)	0.1744(4)	1.59(9)
Si_8	0.15664(4)	0.08573(4)	0.80730(8)	1.04(3)	0.1570(2)	0.0872(2)	0.8103(4)	1.49(8)
Si_9	0.34185(4)	0.09519(4)	0.17376(8)	1.00(2)	0.3417(2)	0.0940(2)	0.1776(4)	1.26(8)
Si_{10}	0.34083(4)	0.08800(4)	0.81013(8)	1.01(2)	0.3405(2)	0.0898(2)	0.8132(4)	1.34(8)
Si_{11}	0.12431(6)	0	1/2	0.88(3)	0.1234(5)	0	1/2	1.07(15)
Si_{12}	0.37491(6)	0	1/2	1.04(3)	0.3735(5)	0	1/2	1.05(14)
Si_{13}	0.25235(4)	1/2 – x	1/4	0.80(3)	0.2509(1)	=1/2 – x	1/4	1.16(8)
O_1	0.0360(2)	0.1788(2)	0.2610(4)	3.19(9)	0.0403(6)	0.1835(6)	0.2590(12)	3.7(3)
O_2	0.0611(2)	0.1844(2)	0.7492(3)	2.73(8)	0.0544(6)	0.1856(6)	0.7448(11)	4.2(3)
O_3	0.0717(2)	0.1149(2)	0.3878(3)	2.80(9)	0.0690(6)	0.1172(4)	0.3895(8)	3.0(3)
O_4	0.0679(2)	0.1376(2)	0.5786(3)	2.33(7)	0.0667(6)	0.1316(5)	0.5887(11)	4.7(4)
O_5	0.1155(2)	0.2005(2)	0.3615(3)	2.87(8)	0.1161(4)	0.2041(5)	0.3632(10)	3.1(3)
O_6	0.1351(2)	0.2032(2)	0.6307(3)	2.73(8)	0.1254(6)	0.2075(5)	0.6365(11)	4.5(3)
O_7	0.3165(2)	0.0507(2)	0.2328(3)	3.64(10)	0.3202(6)	0.0503(6)	0.2383(13)	4.6(4)
O_8	0.3196(2)	0.0456(2)	0.7390(4)	3.41(10)	0.3211(6)	0.0484(6)	0.7394(11)	3.8(3)
O_9	0.3831(2)	0.0736(2)	0.1000(3)	2.78(8)	0.3764(5)	0.0725(6)	0.0909(10)	4.6(4)
O_{10}	0.3655(2)	0.0631(2)	0.9071(3)	2.50(8)	0.3659(4)	0.0645(5)	0.9064(10)	3.1(3)
O_{11}	0.3001(2)	0.1234(2)	0.1103(3)	2.26(7)	0.3025(5)	0.1280(5)	0.1231(10)	3.3(3)
O_{12}	0.2969(2)	0.1242(2)	0.8436(3)	3.87(11)	0.3011(6)	0.1267(6)	0.8540(12)	4.8(4)
O_{13}	0.1584(2)	0.0116(2)	0.4051(3)	2.92(9)	0.1561(5)	0.0074(5)	0.4025(10)	4.0(3)
O_{14}	0.3406(2)	0.0157(2)	0.4068(3)	2.42(8)	0.3382(5)	0.0113(5)	0.4090(10)	3.2(3)
O_{15}	0.0468(2)	0.0897(2)	0.0235(3)	2.30(8)	0.0495(5)	0.0915(6)	0.0141(10)	4.1(3)
O_{16}	0.4539(2)	0.0907(2)	– 0.0313(3)	1.96(7)	0.4560(5)	0.0897(6)	– 0.0211(9)	3.5(3)
O_{17}	0.2632(1)	0.2103(1)	0.1595(3)	1.64(6)	0.2578(6)	0.2072(3)	0.1694(6)	3.6(3)
O_{18}	0.2396(2)	0.1968(1)	0.7892(3)	2.05(7)	0.2452(8)	0.1986(3)	0.8049(6)	4.8(3)
O_{19}	0.0802(2)	0	0	2.03(11)	0.0774(6)	0	0	1.4(3)
O_{20}	0.4226(2)	0	0	1.66(10)	0.4202(11)	0	0	4.0(5)
O_{21}	0.2500(2)	0.1750(1)	– 0.0199(2)	1.49(6)	0.2533(8)	0.1721(3)	– 0.0101(5)	2.0(2)
O_{22}	– 0.0069(2)	0.2496(2)	0.1573(3)	2.03(7)	-0.0049(3)	0.2532(7)	0.1574(4)	2.3(2)
O_{23}	0.1179(2)	0.1316(2)	0.2205(3)	2.69(8)	0.1186(5)	0.1267(6)	0.2340(9)	4.1(3)
O_{24}	0.3667(2)	– 1/2 – x	1/4	3.16(9)	0.3686(5)	=1/2 – x	1/4	4.1(3)
O_{25}	0.1176(2)	– 1/2 – x	1/4	3.58(10)	0.1248(7)	=1/2 – x	1/4	6.1(4)
$M^{14}(1)$	0	0	1/4	67(4)	0	0	1/4	37(1)
$M^{14}(2)$	0	1/2	1/4	26(2)	0	1/2	1/4	37(4)
$M^{14}(3)$	0.2454(9)	0.1228(6)	0.5107(13)	26(1)	0.251(7)	0.1229(9)	0.510(3)	33(2)
M^{12}	0.2504(5)	0	0	6.8(4)	0.245(5)	0	0	11(1)

[*1] Upper and lower lines for refinements based on $Pm\bar{3}n$ and $P\bar{4}3n$, respectively.
[*2] Refinements with $Pm\bar{3}n$.
[*3] Refinements with $P\bar{4}3n$.

Table 4. (Continued.)

			84°C	
atom	*x*	*y*	*z*	B_{eq}(Å^2)
Si_1 *1	0	0.31008(7)	0.11414(7)	1.71(2)
	- 0.0001(4)	0.31013(7)	0.11418(7)	1.73(5)
Si_2 *2	0.18257(5)	= *x*	= *x*	1.73(1)
Si_{21} *3	0.1833(3)	= *x*	= *x*	1.71(6)
Si_{22} *3	- 0.1817(3)	= *x*	= *x*	1.65(6)
Si_3 *1	1/4	0	1/2	1.23(3)
	1/4	0	1/2	1.25(4)
O_1 *2	0.0964(2)	0.2466(2)	0.1348(2)	5.02(8)
O_{11} *3	0.0974(8)	0.2512(8)	0.1364(9)	5.2(3)
O_{12} *3	- 0.0954(8)	- 0.2419(7)	- 0.1344(8)	4.7(3)
O_2 *1	0	0.4063(3)	0.1812(3)	5.5(2)
	- 0.0150(9)	0.4057(3)	0.1820(3)	4.5(2)
O_3 *1	0.3435(3)	0	0	2.7(1)
	0.3432(3)	0	0	2.7(2)
O_4 *1	1/4	1/4	1/4	5.47(9)
	0.2522(10)	= *x*	= *x*	5.58(10)
M^{12} *1	0	0	0	15.4(3)
	0	0	0	15.4(4)
M^{14} *1	1/4	1/2	0	37.2(11)
	1/4	1/2	0	37.2(10)

(2006), the highest symmetry, space group $Pm\bar{3}n$, is ideal symmetry, if the atoms occupy all the minima equally. As already noted, the refinements on space group $Pm\bar{3}n$ were successful at all three temperatures resulting in Si-O bond distances, which were corrected to reasonable values taking highly anisotropic and large MSDs of O atoms into consideration, as shown later. It is reasonable to conclude that the β-phase nearly attains the ideal state. The *R*-values (see Table 3) and the results of the refinements (Tables 4 and 5) using space group $P\bar{4}3n$ are also given for a reference in the case of $T = 84$ °C.

RESULTS AND DISCUSSION

Temperature dependence of the unit cell dimensions

The unit cell dimension, *a*, appears to increase gradually with increasing temperature, including a weak bend at the α-β transition point, up to a temperature of 500 °C (Fig. 1). On the other hand, the value of 2*c*, which is smaller than *a* in the α-phase, rises steeply up to the value of *a* at the transition point. The temperature dependence of the *c*-axis dimension in α-MEP bears a striking resemblance to that observed for quartz. In both structures, the rate of increase in the cell dimensions is smaller at lower temperatures, but increases as the temperature approaches the transition point. In the β-phase, the cubic unit cell dimension weakly increases up to its maximum at about 500 °C, and then begins to contract with increasing temperature. However, this contraction does not mean that the guest molecules are liberated at this temperature. Nakagawa's measurements on a guest-free single-crystal, show that the liberation of guest molecules leads to an expansion of the cell. Nakagawa (2002) showed that guest-free MEP prepared by heating a sample from Mt. Hamilton at 1000 °C exhibits a $Pm\bar{3}n$ space group at room temperature (different from the orthorhombic *Pmmm* space group suggested by Liu et al. (1997) in an NMR study), and the cell constant is about 0.02 Å larger than that of guest-bearing MEP at temperatures between 50 and 200 °C. Our preliminary molecular dynamics simulations are in good agreement with Nakagawa's measurements, indicating that guest-free MEP has a larger cubic unit cell than guest-bearing MEP. (Nakagawa's data is reasonably interpreted as being due to van der Waals interactions between guest molecules and the framework atoms reducing the voids to stabilize the framework.) The decrease in cell dimensions commencing at $T = 500$ °C may be ascribed to increasing thermal vibrational amplitudes with increasing temperature, and is similar to the contraction observed in β-quartz (Kihara, 2001a, 2001b).

Atomic mean-square displacements

At all the temperatures examined, the magnitude of the MSDs of Si was much smaller than that of the O atoms, and no anisotropy was observed. The magnitude was about the same as that in the direction of *Axis-3* of the thermal ellipsoids of the O atoms. (The principal axes of thermal ellipsoid are represented using *Axis-1* for the largest MSD, *Axis-2* for the second largest MSD, and *Axis-3* for the smallest MSD.) In contrast, the thermal ellipsoids of the O atoms are highly anisotropic, particularly for Groups O_1 (O_1-O_{12}), O_2 (O_{13}-O_{18}), and O_4 (O_{23}-O_{25}). The anisotropic MSDs of the O atoms (Fig. 3) appear to share characteristic features with other silicas, especially in the orientation relationship between the principal axes and the Si-O-Si bonding planes. In quartz for example, low frequency rigid librational motion of the Si-O-Si bonds around the Si-Si axes contribute strongly to the MSDs of the O atoms in Axes-1 of thermal ellipsoids, which are orientated nearly perpendicular to the corresponding Si-O-Si planes (Young, 1962). However, in a molecular dynamics simulation of quartz (Kihara, 2001a), another type of thermal disturbance related to atom disorder over Dauphiné twin related positions (separated about 0.8 Å at the O atom-site) is observed at each O-atom site. This type of motion is in the same symmetry (irreducible representation) as the librational motion in a phonon mode (known as the soft mode of the transition), and does

Table 5. Si–O distances and Si–O–Si angles

(a) Si–O distances (Å). Estimated standard deviations are shown in parentheses.

α-melanophlogite					β-melanophlogite			
SiO_4	- 50 (°C)	25 (°C)	40 (°C)	60 (°C)	SiO_4	84 (°C)	100 (°C)	200 (°C)
Si_1	1.590(2)	1.590(4)	1.580(4)	1.600(4)				
Si_2	1.589(2)	1.588(4)	1.595(4)	1.574(4)				
Si_3	1.595(2)	1.583(3)	1.595(4)	1.583(3)	Si_1	1.578(3)	1.580(3)	1.580(2)
Si_4	1.599(2)	1.604(3)	1.591(3)	1.593(3)	Si_1*	1.577(4)	1.588	1.585
Si_5	1.596(2)	1.595(3)	1.592(3)	1.580(3)				
Si_6	1.594(2)	1.585(3)	1.588(3)	1.587(3)				
Mean	1.594(2)	1.591(2)	1.590(2)	1.586(2)				
Si_7	1.592(2)	1.579(4)	1.586(4)	1.593(4)				
Si_8	1.591(2)	1.593(4)	1.588(4)	1.594(4)	Si_2	1.573(3)	1.570(3)	1.570(3)
Si_9	1.588(2)	1.578(3)	1.581(3)	1.568(3)	Si_{21}*	1.597(6)	1.586	1.599
Si_{10}	1.589(2)	1.578(4)	1.578(4)	1.567(4)	Si_{22}*	1.543(6)	1.554	1.546
Mean	1.590(2)	1.582(2)	1.583(2)	1.580(2)				
Si_{11}	1.599(2)	1.571(4)	1.582(4)	1.588(4)				
Si_{12}	1.601(2)	1.606(3)	1.593(3)	1.568(3)	Si_3	1.560(4)	1.561(4)	1.570(4)
Si_{13}	1.593(2)	1.585(3)	1.584(3)	1.578(3)	Si_3*	1.573(5)	1.585	1.576
Mean	1.594(2)	1.587(2)	1.587(2)	1.578(2)				

Entries for Si_1 to Si_{13} are averages over corresponding SiO_4 tetrahedra.
Si atoms in α-melanophlogite are divided into three or four groups for $Pm\bar{3}n$ or $P\bar{4}3n$, respectively, in β-melanophlogite, each becomes Si_1, Si_2 and Si_3 or Si_1, Si_{21}, Si_{22} and Si_3.
* $P\bar{4}3n$ cases, shown only for 84 °C.

(b) Si–O–Si angles (°).

α-melanophlogite*1					β-melanophlogite*2			
O_1 - O_{12}	169(7)	161(5)	162(6)	163(6)	O_1	165.9(2)	165.9(2)	166.1(3)
					O_{11}*3	165.9(8)		
					O_{12}*3	165.8(8)		
O_{13} - O_{18}	156(6)	160(6)	161(6)	165(4)	O_2	178.6(3)	178.6(3)	178.7(3)
					O_2*3	165.5(3)		
O_{19} - O_{22}	148(3)	148(3)	147(3)	148(1)	O_3	147.4(4)	147.5(3)	147.6(1)
					O_3*3	147.6(4)		
O_{23} - O_{25}	161(4)	166(5)	167(7)	171(8)	O_4	180	180	180
					O_4*3	180.0(9)		
Mean	157	159	160	162	Mean*4	168	168	169

*1 Each entry for α-melanophlogite is an unbiased estimate of average, $\overline{Si\text{–}O\text{–}Si}$, over angles for O atoms indicated, which become O_1 to O_4 in β-melanophlogite, and $\hat{\sigma}(\overline{Si\text{–}O\text{–}Si})$, estimate of the standard deviation of $\overline{Si\text{–}O\text{–}Si}$, in parentheses.
*2 Values in parentheses are estimated standard deviations in the refinements.
*3 $P\bar{4}3n$ cases, shown only for 84 °C.
*4 Mean for the case of $Pm\bar{3}n$.

not cause any notable distortion of the Si–O–Si bond. In other words, the librational motion can trigger or boost the transfer motion through the possible coupling between them.

Figure 4 shows the temperature dependence of the MSDs of Axes–1, –2, and –3 of the thermal ellipsoids for each of the four groups of O atoms in MEP. The averages were taken over O_1–O_{12} for Group O_1, O_{13}–O_{18} for Group O_2, O_{19}–O_{22} for Group O_3, and O_{23}–O_{25} for Group O_4. It is noted that the MSDs for the O atoms in Axes–1 and –2 increase with increasing temperature up to the transition point, after which, they remain constant or show a tendency to decrease. The increase in Axis–1 of O_2 is especially notable. It begins at a temperature of about 15 °C below the transition temperature. On the other hand, the MSD curves of Axis–3 for all the groups of O atoms in MEP remain low, nearly equal to 0.02 $Å^2$, at temperatures below 200 °C. The temperature dependence of the MSDs along the three axes again bear striking resemblances to those observed in quartz, except for the steep increase in

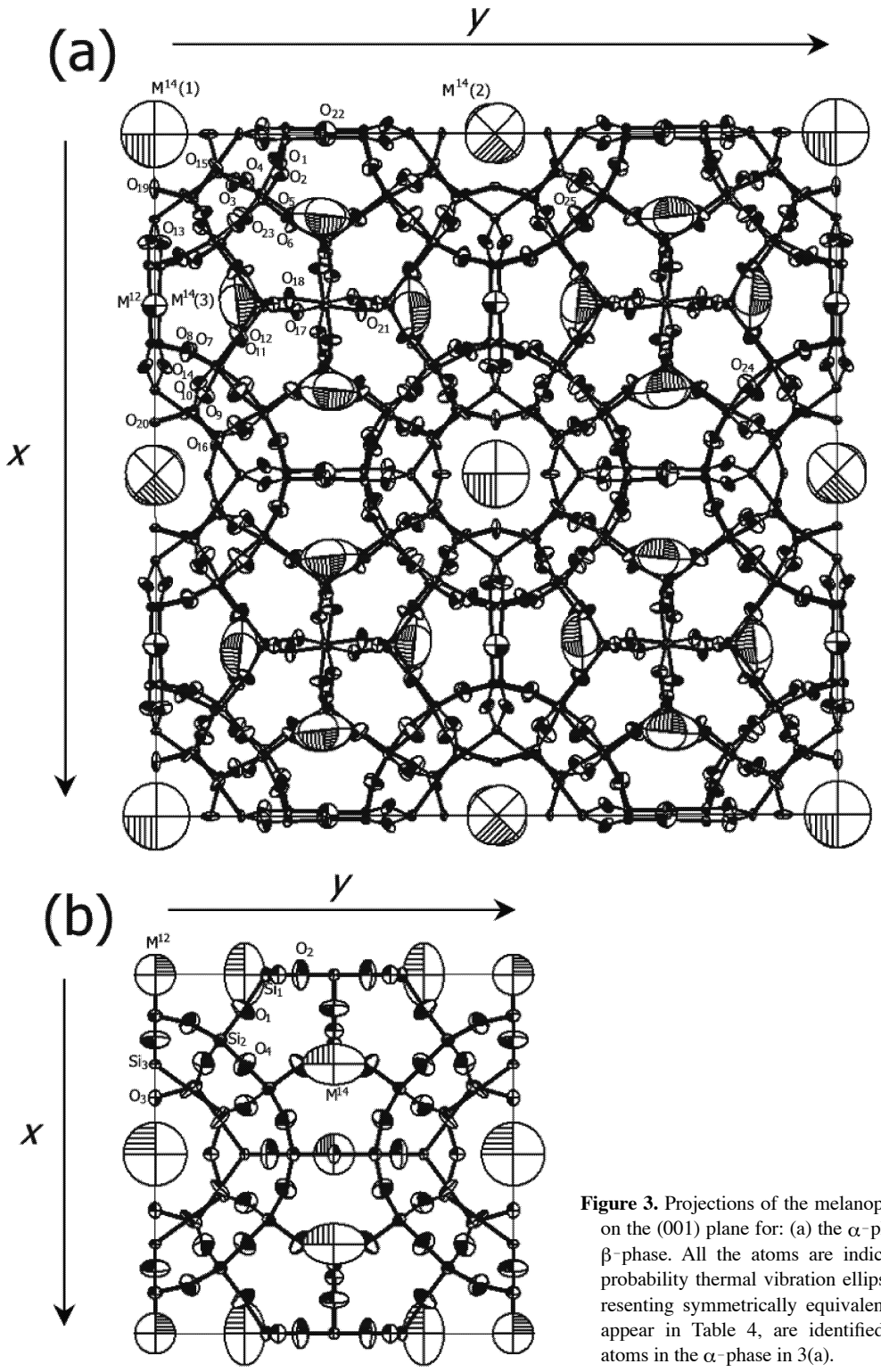

Figure 3. Projections of the melanophlogite structure on the (001) plane for: (a) the α-phase, and (b) the β-phase. All the atoms are indicated for a 50% probability thermal vibration ellipsoid. Atoms representing symmetrically equivalent groups, which appear in Table 4, are identified, except for Si atoms in the α-phase in 3(a).

MSDs along Axis-1 of the O_2 group of atoms up to 0.13 Å^2 at T = 84 °C, which is much larger than those in β-quartz at T = 575 °C (Kihara, 1990).

Structural changes in melanophlogite

The librational motion of the Si-O-Si bonding plane, as considered by Young (1962) for quartz, in which the atoms move in one of the energy minima, may be inadequate to cause such large magnitude MSDs in MEP at

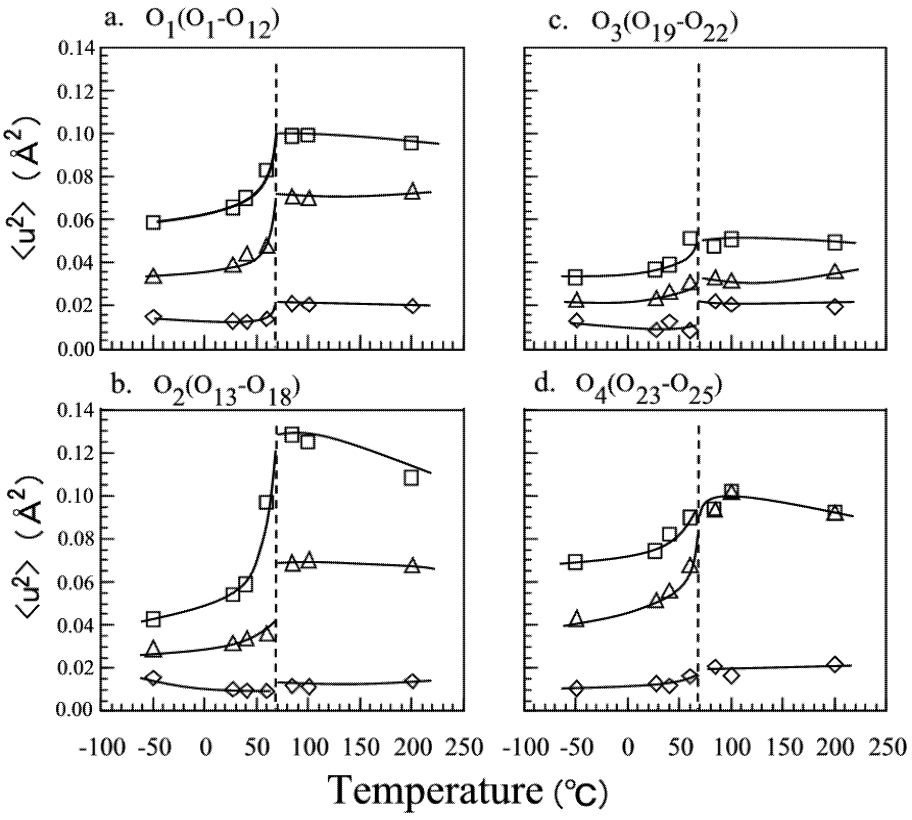

Figure 4. Temperature dependence of the mean-square displacement ($<u^2>$ Å^2) of the O atoms along the principal axes of the thermal ellipsoids. The atom temperature factors are taken from the least-squares refinement for the $P4_2/nbc$ space group for the α-phase and the $Pm\bar{3}n$ space group for the β-phase. The vertical broken lines show the approximate α-β transition point. The solid lines are provided for visual guidance only. Key: Squares, Axis-1; Triangles, Axis-2; Diamonds, Axis-3. a: the O_1 group (O_1 to O_{12}). b: the O_2 group (O_{13} to O_{18}). c: the O_3 group (O_{19} to O_{22}). d: the O_4 group (O_{23} to O_{25}).

temperatures as low as 84 °C. According to Nakagawa and Kihara (2006), the framework atoms in β-MEP are possibly disordered over twelve potential energy minima per atom site. A type of motions similar to the transfer motions, observed in the molecular dynamics simulation of quartz, may also occur over some of those 12 energy minima at each atom site in α-MEP. With increasing temperatures, the transfer becomes more frequent, and involves more energy minima at each site. Finally the structure attains the higher symmetry, in which the transfer motions occur so frequently throughout the entire crystal that all the potential energy minima are equally occupied by atoms in a statistical sense. The MSDs mostly remain unchanged above the transition point, because the structure attains a state in which all the available minima are equally occupied.

The characteristic temperature dependences of the MSDs and unit-cell dimensions strongly suggests that the α-β transition in MEP advances via a mechanism similar to that in quartz. However, the simple coupling mechanism between librations (of a phonon mode) and transfer motions, assumed for quartz, cannot be directly applied to MEP, because the structure is more complicated with four different types of O site (each O site has a unique PDF). Then, we only consider here that 12 minima are available at each atom site in MEP, and those are dynamically occupied: averaged occupancy over crystal and time is 1/12 for each minimum in β-MEP to achieve the highest symmetry $Pm\bar{3}n$, and not so in α-MEP, in which occupancy at each minimum changes toward 1/12 with increasing temperature. More details about the α-β transition mechanism are given in Nakagawa and Kihara (2006).

As already indicated, the temperature evolutions of the intensities of the superstructure-reflections are successfully fitted with an equation for first-order phase transitions. However, the results, i.e., $T_c \sim T_o$ and small jumps at T_c may suggest rather a tricritical nature. These α-β transition mechanism in quartz and MEP are apparently different from those observed between the tetragonal and cubic phases in cristobalite (Peacor, 1973; Schmahl et al., 1992) or between monoclinic (MC) and orthorhombic (OP) tridymite (Hirose et al., 2005), in which the unit-cell dimensions and atom MSDs show a small, linear temperature dependences up to the transition point. According to Hirose et al. (2005), no effects due to of disorder were observed in the MC phase of tridymite, even at temperatures just below the transition point.

Temperature dependence of the Si-O bond distance and Si-O-Si bond angle

The positional parameters of the atoms in α-MEP change

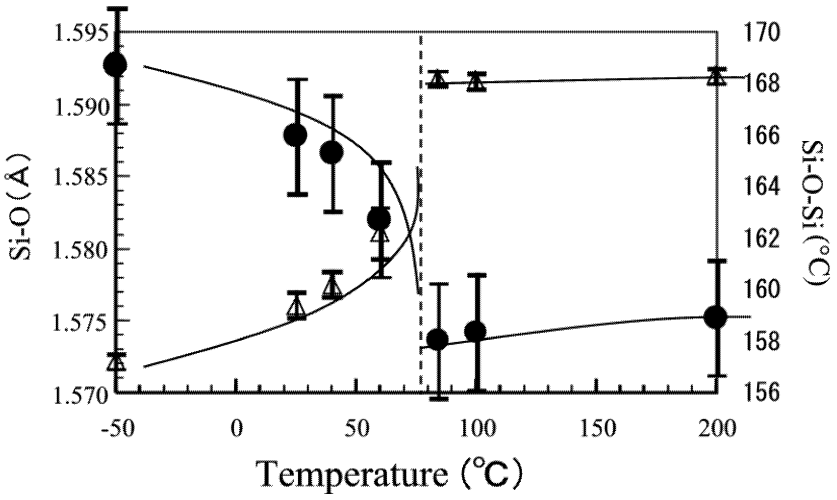

Figure 5. Temperature dependence of the average Si-O bond distance and Si-O-Si bond angle. The atomic coordinates are taken from those obtained from least-squares refinement of the $P4_2/nbc$ space group for the α-phase and the $Pm\bar{3}n$ space group for the β-phase. Key: Solid circles, Si-O (Å); Open triangles, Si-O-Si (°). The error bars denote the 2σ values. The vertical broken line shows the approximate α-β transition point. The lines are provided for visual guidance only.

Table 6. Δ_{Si-O} criteria used in a rigid body motion analysis of α- and β-melanophlogite

	Δ_{Si-O}*		
α-phase	25 ℃	40 ℃	60 ℃
Si_1	0.00056	- 0.00045	0.00121
Si_2	- 0.00062	- 0.00041	- 0.00129
Si_3	0.00009	- 0.00086	- 0.00857
Si_4	0.00159	0.00055	0.00644
Si_5	0.00138	- 0.00142	- 0.00278
Si_6	0.00374	0.00134	- 0.00123
Si_7	0.0016	- 0.00257	- 0.00314
Si_8	- 0.00074	- 0.00064	- 0.00939
Si_9	0.00143	0.00226	0.0023
Si_{10}	0.00338	0.00368	0.00903
Si_{11}	- 0.00032	0	0.00399
Si_{12}	0.00177	- 0.00143	- 0.00935
Si_{13}	0.00126	- 0.00253	- 0.00183
Mean	0.00107	- 0.00033	- 0.00095
β-phase	84 ℃	100 ℃	200 ℃
Si_1	- 0.00022	- 0.00069	0.00003
Si_2	- 0.00042	- 0.00067	0
Si_3	- 0.00285	- 0.00327	- 0.00132
Mean	- 0.00063	- 0.00102	- 0.00016

* $\Delta_{Si-O} = \langle u_v^2 \rangle_O - \langle u_v^2 \rangle_{Si}$, where $\langle u_v^2 \rangle$ is atomic mean-square displacements along Si-O bonding directions.

gradually compared to those in β-MEP (see Table 4), which remain nearly constant up to a temperature of 200 °C. Figure 5 shows the temperature dependence of both the Si-O bond length and the Si-O-Si bond angle, averaged over all pairs and triplets. The Si-O bond lengths and Si-O-Si bond angles either increase or decrease with increasing temperature up to the transition point, after which, both the quantities show only a weak temperature dependency. The negative temperature dependence of the Si-O bond length in α-MEP is noticeable. The Si-O-Si bonding planes in MEP must undergo librational motions around the Si-Si axes, and, in addition, the disorder increases with increasing temperature, involving more energy minima at every atom site.

Table 7. Corrected Si-O bond lengths

Temperature (°C)	Corrected (Å)	Uncorrected (Å)
- 50	1.611	1.592
25	1.610	1.588
40	1.610	1.587
60	1.611	1.583
84	1.610	1.571
100	1.613	1.574
200	1.613	1.575

Note: Downs et al. (1990)'s *simple rigid bond* analysis was applied to Si-O distances calculated for atomic mean positions.

In our harmonic refinement, the real PDFs for the O atoms involving all such effects were constrained to be anisotropic. The inter-mean distance (the distance between the mean of the PDFs) became shorter than the real bond length with increased amplitude of libration (Willis and Pryor, 1975), or increased anisotropic MSDs due to the disorder. A quantity was calculated as follows

$$\Delta_{Si-O} = \langle u_v^2 \rangle_O - \langle u_v^2 \rangle_{Si},$$

Where $\langle u_v^2 \rangle$ denotes the magnitude of $\langle u^2 \rangle$ in the Si-O bond direction. These are listed in Table 6, and ensure that the Si-O bond in MEP was kept rigid during any thermal disturbance.

We attempted to carry out a bond distance correction using Downs et al.'s (1990) *simple rigid bond* analysis, which employs a model of rigidly coordinated polyhedra with the central cations undergoing only translational motion, and the corrected Si-O bond distances are shown in Table 7. The corrected values show no significant temperature dependence at a bond distance of about 1.611 Å, which is in excellent agreement with other common silica

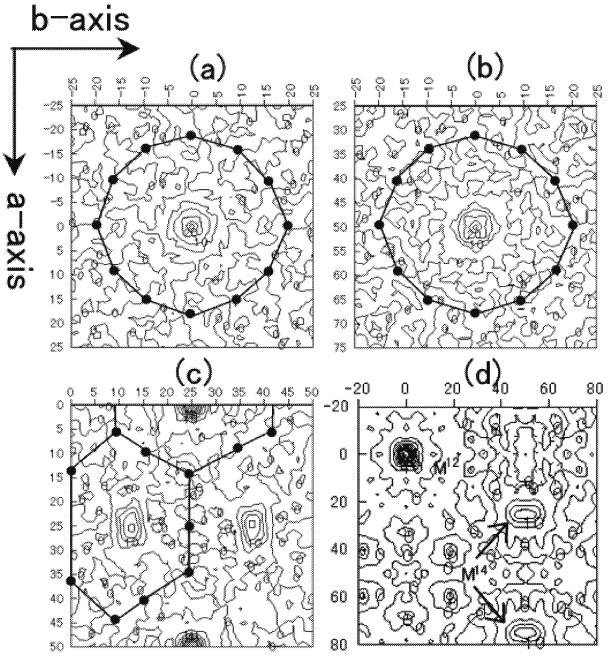

Figure 6. Difference Fourier maps, $\rho_{obs} - \rho_{calc\ (Si,O)}$. The ($a/2 \times b/2$) sections, including $M^{14}(1)$, $M^{14}(2)$, $M^{14}(3)$, and M^{12}, at 25 °C for α-melanophlogite are shown: (a) x and $y = -0.25$ to 0.25 for $z = 0.25$, (b) $x = 0.25$ to 0.75 and $y = -0.25$ to 0.25 for $z = 0.25$, and (c) x and $y = 0$ to 0.5 for $z = 0.5$. An ($a \times b$) section passing through M^{12} and M^{14} at 84 °C for β-melanophlogite is shown in (d) for x and $y = -0.2$ to 0.8 for $z = 0$. Contour scale = × 10 e/Å^3. In (a), (b), and (c), solid lines are used to join some of the framework Si positions (solid circles), surrounding the void spaces.

structures.

Temperature factors of the M^{12} and M^{14} sites

The temperature factors of the substitute atoms for the cage sites were quite large ($B_{eq} \sim 15$ and 37 Å^2 for M^{12} and M^{14}, respectively, at 84 °C), and were far above a reasonable level for atoms in common solids. This partly arises from our calculations using single scatterers for CH_4, N_2, and CO_2 molecules, but some significant part must arise from real effects, such as Van der Waals interactions between those molecules and the framework atoms. The electrons of the linear molecules, CO_2 or N_2, have much larger distributions than the spherical Mg atom used for the M^{14} site in our refinements. For example, $d_{C\text{-}O} = 1.163$ Å and $d_{N\text{-}N} = 1.10$ Å (Wells, 1975). The use of spherical form factors may cause an increase in the vibrational parameters, particularly for the M^{14} sites. The temperature factors obtained for the M^{12} sites may be less affected using the form factors of a neutral F atom, because the size of CH_4 ($d_{C\text{-}H} \sim 1.1$ Å) and F ($r_F < 1.2$ Å) are not so different from each other, as for the case of Mg and the linear molecules. The increased temperature factor of the M^{12} site may come from real thermal disturbances. The increased space ($d_{M^{12}\text{-}O_1} \sim 3.99$ Å and $d_{M^{12}\text{-}O_3} \sim 4.60$ Å) and weak interactions between the molecules and the framework atoms may allow for larger thermal vibrations.

The voids of the M^{14} sites are oblate spheroidal in shape, with axes perpendicular to the hexagonal rings, through which the cages are linked each other to form pipes of cages aligned parallel with the crystallographic axes (Nakagawa et al. 2001). Figure 6(a, b) shows the electron density of the M^{14} sites obtained from the difference of Fourier synthesis using $F_o - F_{c(Si,O)}$. These all show a single peak around their centers, but exhibit angular distributions, particularly in the section perpendicular to the spheroidal axes. The electron density distribution dominates in the plane perpendicular to the spheroidal axes, where the largest space is available. The largest value of $d_{M^{14}\text{-}O}$ is about 5.1 Å for the O atoms in these planes, compared to the smallest value of 3.95 Å for the hexagonal interfaces. This electron density distribution is consistent with the results obtained from our preliminary molecular dynamics study. The motion of the linear molecules (e.g., CO_2) is dominated by motions with their axes in the plane with the largest space. The electron density of the M^{12} site also exhibits a single peak, and the contour lines are also angular (and rather square-like) (Fig. 6d). Probably the *rigid* guest molecules move to conform to some definite orientation of the potential energy minima, which results in such angular electron density distributions within the constraint of the site symmetry in the pentagondodecahedral or tetrakaidecahedral void. A detailed analysis of the disorder of the guest molecules and their interactions with the SiO_2 framework remain the subject of a future study.

CONCLUDING REMARKS

The α-β transformation in MEP takes places at about 65 °C. The structural changes of the α- to -β transition in MEP are driven by increasing atom disordering over multiple potential energy minima with increasing temperature. The mechanism is comparable to that for quartz, but differs from that for the obvious first-order phase transition between the low temperature phases of tridymite, or between the α- and β-phases of cristobalite. The Si-O bonds are nearly rigid from the viewpoint of related atom MSDs. The large MSDs of the framework O atoms and their temperature dependence are ascribed to the disorder (dynamical or static), which becomes significant at higher temperatures. The Si-O bond distances calculated for related coordinates in our least-squares refinements, and the cell dimensions, show a negative temperature dependence, but this may be due to a strong distortion of the

probability density functions of the O atoms. The Si-O bond distances assuming a rigid body motion are less temperature-dependent, and are about 1.611 Å.

REFERENCES

Becker, P.J. and Coppens, P. (1974) Extinction within the limit of validity of the Darwin transfer equations. I. General formalisms for primary and secondary extinction and their application to spherical crystals. Acta Crystallographica, A30, 129-147.

Cromer, T. and Waber, J.T. (1974) Atomic scattering factors for X-rays. In International Tables for X-ray Crystallography IV (Ibers, J.A. and Hamilton, W.C. Ed.). pp. 366, Kynoch Press, Birmingham, 71-147.

Downs, R.T., Gibbs, G.V. and Boisen, M.B.Jr. (1990) A study of the mean-square displacement amplitudes of Si, Al and O atoms in framework structure: Evidence for rigid bonds, order twinning and stacking faults. American Mineralogist, 75, 1253-1267.

Downs, R.T., Gibbs, G.V., Bartelmehs, K.L. and Boisen, M.B. Jr. (1992) Variations of bond lengths and volumes of silicate tetrahedral with temperature. American Mineralogist, 77, 751-757.

Gies, H. (1983) Studies on clathrasils. III., Crystal structure of melanophlogite, a natural clathrate compound of silica. Zeitschrift für Kristallographie, 164, 247-257.

Gies, H. and Marler, B. (1992) The structure-controlling role of organic templates for the synthesis of porosils in the system SiO_2/template/H_2O. Zeolites, 12, 42-49.

Hatch, D. M. and Ghose, S. (1991) The α-β phase transition in cristobalite, SiO_2. Physics and Chemistry of Minerals, 17, 554-562.

Hirose, T., Kihara, K., Okuno, M., Fujinami, S. and Shinoda, K. (2005) X-ray, DTA and Raman studies of monoclinic tridymite and its higher temperature orthorhombic modification with varying temperature. Journal of Mineralogical and Petrological Sciences, 100, 55-69.

Kamb, B.(1965) A clathrate crystalline form of silica. Science, 148, 232-234.

Kihara, K. (1990) An X-ray study of the temperature dependence of the quartz structure. European Journal of Mineralogy, 2, 63-77.

Kihara, K. (2001a) Molecular dynamics interpretation of structural changes in quartz. Physics and Chemistry of Minerals, 28, 365-376.

Kihara, K. (2001b) Thermal expansions in quartz: A geometrical consideration. Journal of Mineralogical and Petrological Sciences, 96, 159-163.

Kihara, K., Matsumoto, T. and Imamura, M. (1986) High-order thermal-motion tensor analyses of tridymite. Zeitschrift für Kristallographie, 177, 39-52.

Kortus, J., Irmer, G., Monecke, J. and Pederson, M.R. (2000) Influence of cage structures on the vibrational modes and Raman activity of methane. Modelling and Simulation in Materials Science and Engineering, 8, 403-411.

Liu, S., Welch, M.D. and Klinowski, J. (1997) NMR study of phase transitions in guest-free silica clathrate melanophlogite. Journal of Physical Chemistry B, 101, 2811-2814.

Mair, S.L. and Wilkins, S.W. (1981) On the X-ray or neutron diffraction determination of atomic position parameters. Acta Crystallographica, A37, 264-266.

Nakagawa, T. (2002) X-ray single crystal studies of natural melanophlogite. Doctoral thesis, Kanazawa University, Kanazawa, Japan.

Nakagawa, T., Kihara, K. and Harada, K. (2001) The crystal structure of low melanophlogite. American Mineralogist, 86, 1506-1512.

Nakagawa, T. and Kihara K. (2006) A higher order thermal motion tensor analysis of cubic melanophlogite and the disorder of O atoms, in press.

Peacor, D.R. (1973) High temperature single-crystal study of the cristobalite inversion, Zeitschrift für Kristallographie, 138, 274-298.

Schmahl, W.W., Swainson, I.P., Dove, M.T. and Graeme-Barber, A. (1992) Landau free energy and order parameter behaviour of the α/β phase transition in cristobalite. Zeitschrift für Kristallographie, 201, 125-145.

Skinner, B.J. and Appleman, D.E. (1963) Melanophlogite, a cube polymorph of silica. American Mineralogist, 48, 854-867.

TEXSAN™ (1989) Structure solution package. The Rigaku Journal, 6, 43-45.

Wells, A.F. (1975) Structural Inorganic chemistry. pp. 1095, Clarendon Press, Oxford, Great Britain.

Willis, B.T.M. and Pryor, A.W. (1975) Thermal vibrations in crystallography. pp. 280, Cambridge University Press, London, Great Britain.

Wright, A.F. and Leadbetter, A.J. (1975) The structure of the β-cristobalite phases of SiO_2 and $AlPO_4$. Philosophical Magazine, 31, 1391-1401.

Young, R.A. (1962) Mechanism of the phase transition in quartz. Report 2569, pp. 155, Air Force Office Scientific Research, Washington 25, D.C. United States of America.

Žák, L. (1972) A contribution to the crystal chemistry of melanophlogite. American Mineralogist, 57, 779-796.

Manuscript received April 21, 2005
Manuscript accepted August 8, 2005
Manuscript handled by Yasuhiro Kudoh